ICSTI
6th International Congress on the Science and Technology of Ironmaking - ICSTI
42th Ironmaking and Raw Materials Seminar/ 42º Seminário de Redução de Minério de Ferro e Matérias-primas
13th Brazilian Symposium on Iron Ore/ 13º Seminário Brasileiro de Minério de Ferro
ISSN 2176-3135

MODELLING OF IRONMAKING BLAST FURNACE: COMPARISON OF SLOT AND SECTOR GEOMETRIES[1]

Yansong Shen[2]
Baoyu Guo[2]
Peter Austin[3]
Sheng Chew[3]
Aibing Yu[2]

Abstract
In this paper, a mathematical model is developed to describe the complex behaviours of gas-solid-liquid multiphase flow, their heat and mass transfers and chemical reactions in an ironmaking blast furnace. The model is used to investigate and visualise the effects of different model configurations, *viz*. slot vs. sector geometry, on the location/shape of cohesive zone and other key process variables such as velocity, temperature, component concentration of each phase, reduction degree and gas utilization. The comparisons show that predictions of fluid flow and thermo-chemical phenomena using the slot and sector geometries are quite different, ***e.g***. the sector geometry predicts a higher cohesive zone, faster reduction and a lower gas utilization at furnace top. This implies that the model geometry setting is significant when numerically examining the multiphase behaviours inside a blast furnace. The model provides a cost-effective method for understanding and optimizing the blast furnace operation for better stability and productivity.
Key words: Blast furnace; Modelling; Multiphase flow; CFD; Slot; Sector.

[1] *Technical contribution to the 6th International Congress on the Science and Technology of Ironmaking – ICSTI, 42nd International Meeting on Ironmaking and 13th International Symposium on Iron Ore, October 14th to 18th, 2012, Rio de Janeiro, RJ, Brazil.*

[2] *Lab for Simulation and Modelling of Particulate Systems, School of Materials Science and Engineering, University of New South Wales, Sydney NSW 2052, Australia.*
[3] *BlueScope Steel Research, P.O. Box 202, Port Kembla, NSW 2505, Australia.*

ISSN 2176-3135

1 INTRODUCTION

Ironmaking blast furnace (BF) plays a dominant role in iron production worldwide. Practically, the lump solids, *i.e.* iron ore in various forms and coke, are charged from the top of the furnace. Hot air (blast) enters the furnace through the tuyeres into the lower part of BF and combusts coke to form reducing gas. As the solid descends and gas ascends, the gas reduces and melts the iron ore to form liquid iron and slag in the cohesive zone, typically ranging 1,200°C-1,400°C. The liquid then percolates through the coke bed to the hearth.[1,2] If pulverized coal injection is practised at high injection rates, unburnt coal will leave the raceway region and enter the coke bed.[3,4] Physically, the BF is a moving bed reactor involving counter-, co- and cross-current flows of gas, liquid and solid phases, coupled with their heat exchange and chemical reactions, where the three phases affect each other via inter-phase forces and heat transfers.[1,2] All these features show the complexity of BF operation and hence demonstrate the difficulties in understanding and optimizing BF operation. It is therefore desirable to understand the complex in-furnace phenomena for process control and optimization.

In the past decades, various techniques have been used to understand the complex behaviours inside a BF. Industry-scale investigations such as dissection studies and in-situ measurements can only provide limited information for an operating BF. It is difficult to reproduce the in-furnace phenomena in pilot- or laboratory-scale physical experiments due to the high pressure and high temperature environment inside a real BF. As a result, a mathematical approach has been widely used to investigate the internal state of a BF with detailed information about fluid flow, heat and mass transfer, and chemical reactions. In the past, continuum-based and, more recently, discrete-based mathematical models have been developed in one-, two- and three-dimensions, as summarized in recent review papers.[5,6] The particle number in a practical BF is huge and thus computational cost is very expensive for discrete-based BF models. For this reason, continuum-based BF models are the major modelling technique used to describe and characterise the internal state of a BF,[5] with slot and sector model geometry settings adopted by different researchers. It is therefore necessary to understand the influences of these different model geometry settings on BF predictions, in particular the location and shape of the cohesive zone.

In this paper, in order to simulate the internal state of a BF and understand/visualize the effects of different model geometries on process variables, a CFD model will be developed to describe the complex behaviours of gas-solid-liquid multiphase flow and their heat/mass transfers and chemical reactions in a BF. The effect of different model configurations, *i.e.* slot vs. sector geometry settings, on BF simulations will be compared, in terms of cohesive zone location and other key process parameters such as velocity, temperature, component concentration, reduction degree and gas utilization.

2 MODEL DESCRIPSION

This model will cover the physico-chemical phenomena in a BF in aspects of flow and thermo-chemical behaviours of gas-solid-liquid phases, the heat-mass-momentum transfer between the phases, oxidation/reduction reactions, and consequential phase changes. The model formulation is outlined below. The model is developed based on the ANSYS-CFX CFD software package.[7] Specifically, the Eulerian multicomponent- multiphase module of CFX is used in this model. This

ISSN 2176-3135

platform was chosen for easy transfer from academia to industry and potential connection with previous submodels.[4,8]

2.1 Governing Equations

The governing equations describing the fluid flow, heat and mass transfer, and chemical reactions are listed in Table 1. The gas phase flow is described by the well-established Navier-Stokes equations[9] through porous media. Solids are assumed as a continuous phase through porous media (gas and liquids), and modelled using the so-called viscous model.[10] Liquids are treated as a single phase of discrete rivulets or droplets under the influence of gravity, gas drag and bed resistance, and modelled by the so-called force balance approach.[11,12] The three phases exchange data via a shared library.

Table 1. Governing equations used in the BF model

		Governing equations
Mass		$\nabla\cdot(\varepsilon_i\rho_i\mathbf{U}_i)=S_i$, where $S_i=-\sum_k\beta_{i,k}R_k^*$
Momentum	Gas	$\nabla\cdot(\varepsilon_g\rho_g\mathbf{U}_g\mathbf{U}_g)=\nabla\cdot\tau_g-\varepsilon_g\nabla p+\rho_g\varepsilon_g\mathbf{g}+\mathbf{f}_g^{s}+\mathbf{f}_g^{l,d}$ $\boldsymbol{\tau}_g=\varepsilon_g\mu_g[\nabla\mathbf{U}_g+(\nabla\mathbf{U}_g)^T]-2/3\varepsilon_g\mu_g(\nabla\cdot\mathbf{U}_g)\mathbf{I}$
	Solid	$\nabla\cdot(\varepsilon_s\rho_s\mathbf{U}_s\mathbf{U}_s)=\nabla\cdot\tau_s-\varepsilon_s\nabla p_s+\rho_s\varepsilon_s\mathbf{g}$ $\boldsymbol{\tau}_s=\varepsilon_s\mu_s[\nabla\mathbf{U}_s+(\nabla\mathbf{U}_s)^T-2/3\varepsilon_s\mu_s(\nabla\cdot\mathbf{U}_s)\mathbf{I}$
	Liquid	$\mathbf{f}_{l,d}^{g}+\mathbf{f}_{l,d}^{s}+\varepsilon_{l,d}\rho_l\mathbf{g}=0$
Heat and species		$\nabla(\varepsilon_i\rho_i\mathbf{U}_i\phi_{i,m})-\nabla(\varepsilon_i\Gamma_i\nabla\phi_{i,m})=S_{\phi_{i,m}}$
Volume fraction		$\sum_i\varepsilon_i=1$
State equation for gas phase		$p=\sum_i(y_iM_i)RT_g/V_g$

2.2 Inter-Phase Transfers and Chemical Reactions

The empirical correlations used for calculating the interaction forces between phases are listed in Table 3. Table 3 lists the key chemical reactions considered in this model and the expressions used to calculate the reaction rates. Note that these tables only outline the main equations and expressions with their reference information. The inter-phase heat transfers are available elsewhere[1] and are not listed here due to space limitations. In addition, the main concern of this study is the relative effects of slot and sector geometries on cohesive zone location and thus the interphase heat transfer for liquid phase is not considered for simplicity.

ISSN 2176-3135

Table 2. Empirical correlations for the interaction forces between phases

Phases	Interaction forces	Ref.
Gas-solid	$\mathbf{f}_g^s = -\mathbf{f}_s^g = -(\alpha_f \rho_g \left\|\mathbf{U}_g^s\right\| + \beta_f)\mathbf{U}_g^s$	[5]
Gas-liquid	$\mathbf{f}_g^{l,d} = -\mathbf{f}_{l,d}^g = -\left(\frac{h_{l,d}}{d_l} + \frac{A_{sl,d}}{6}\right)\left[150\left(\frac{\varepsilon_s + h_{l,t}}{d_w}\right)\mu_g + 1.75\rho_g\left\|\mathrm{U}_g\right\|\right]\frac{\mathbf{U}_g}{\varepsilon_g}$	[12]
Liquid-solid	$\mathbf{f}_{l,d}^s = \left(\frac{150}{36}\mu_l \frac{A_{sl,d}^2}{h_{l,d}^2} + \frac{1.75}{6}\rho_l \frac{A_{sl,d}}{h_{l,d}}\left\|\mathbf{U}_l\right\|\right)\mathbf{U}_l$	[12]

Table 3. Reaction rate of key chemical reactions considered in the model

Reaction	Reaction rate	Ref.
$Fe_2O_{3(s)} + CO_{(g)} \rightarrow Fe_{(s)} + CO_{2(g)}$	$R_1 = \frac{N_{ore}\pi {d_{ore}}^2 {\phi_{ore}}^{-1}\rho_g\left[K/(1+K)\right]\left[\xi_{CO} - \xi_{CO_2}/K(M_{CO}/M_{CO_2})\right]}{{k_f}^{-1} + 0.5d_{ore}[(1-f_s)^{-1/3} - 1]D_j^{-1} + [(1-f)^{2/3}k_1(1+1/K)]^{-1}}$	[1]
$FeO_{(l)} + C_{(s)} \rightarrow Fe_{(l)} + CO_{(g)}$	$R_2 = k_2 A_c / (V_b a_{FeO})$	[1]
$CO_{2(g)} + C_{(s)} \rightarrow 2CO_{(g)}$	$R_3 = f(d_{coke})h(S_L)\frac{E_f \rho_s \xi_{coke}\overline{M}_g}{3600M_{coke}}\frac{k_1 p_T \xi_{CO_2}}{1 + p_T(k_2 y_{CO_2} + k_3 y_{CO} + k_5 y_{H_2O})}$	[13]
$FeO_{(s)} \rightarrow FeO_{(l)}$ $Flux_{(s)} \rightarrow Flux_{(l)}$	$R_4 = \left\langle \frac{T_i - T_{\min,sm}}{T_{\max,sm} - T_{\min,sm}} \right\rangle_0^1 \frac{\oint \xi_{sm}\mathbf{U}_i \rho_i \varepsilon_i dA}{M_{sm} Vol_{cell}}$	[14]

2.3 Simulation Conditions and Treatments

2.3.1 Simulation conditions

In this study, the model is applied to a BF of height 25 m, throat diameter 6.4 m, belly diameter 8.8 m and hearth diameter 7.2 m (Figure 1), similar to that used in our previous study.[15] The steady-state model is in two dimensions using a half BF geometry, where the slot configuration is 0.1 m in thickness and the sector configuration covers an arc of 4 degrees. The coke consumption rate in the BF is naturally determined by the reactions considered in the model. The main simulation conditions used in this study are listed in Table 4. The physical and chemical properties of each component in the three phases can be found elsewhere[15,16] and are not repeated here due to space limitations.

ISSN 2176-3135

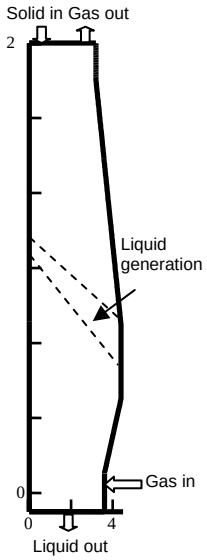

Figure 1. Computational domain with inlet/outlet conditions indicated for each phase.

Table 4. Simulation conditions and operational conditions used in the model

Operational conditions	Variables and values
Gas	
Mass flowrate, $kg \cdot m^{-2} \cdot s^{-1}$	11.7
Volume flux, $Nm^3\ tHM^{-1}$	1511
Inlet gas components, molar pct	34.95 CO; 65.05 N_2
Inlet gas temperature, ℃	2040
Top pressure, atm	2.0
Solid	
Total solid loading, $kg\ m^{-2}\ s^{-1}$	1.22
Ore, $t\ tHM^{-1}$	1.64
Ore components, mass fraction	Fe_2O_3 0.656; FeO 0.157
Ave. ore particle size, m	0.03
Coke, $t\ tHM^{-1}$	0.5023
Coke components, mass fraction	C 1.0
Ave. coke particle size, m	0.045
Ore voidage	$0.403(100d_{ore})^{0.14}$
Coke voidage	$0.153\log d_{coke}+0.724$
Ave. ore/(ore+coke) volume ratio	0.5923
Liquid	
Components, mass fraction	C 0.04;; Fe 0.9509
Density, $kg\ m^{-3}$	6600
Viscosity, $kg\ m^{-1}\ s^{-1}$	0.005
Conductivity, $W\ m^{-1}\ K^{-1}$	28.44
Surface tension, $N\ m^{-1}$	1.1
Slag rate, $t\ tHM^{-1}$	0.377
Density, $kg\ m^{-3}$	2600
Viscosity, $kg\ m^{-1}\ s^{-1}$	1.0
Conductivity, $W\ m^{-1}\ K^{-1}$	0.57
Surface tension, $N\ m^{-1}$	0.47

2.3.2 Treatment of burden

At the furnace top, in the slot geometry, the volume ratio of ore/(ore+coke) is assumed to change linearly from 0.4 at the furnace centre to 0.8 at the wall; the ore particle size is assumed to be constant at 0.03 m while coke particle size is assumed

ISSN 2176-3135

to change linearly with the ore/(ore+coke) volume ratio, from 0.06 m at the centre to 0.03 m at the wall. In the sector geometry, the volume ratio of ore/(ore+coke) is also assumed to change from 0.4 at the furnace centre to 0.8 at the wall, with a quadratic relationship used to make sure the total batch weight ratio is the same as that used in the slot geometry; the ore particle size is assumed to be constant at 0.03 m and coke particle size is assumed to change from 0.06 m at the centre to 0.03 m at the wall. It is noted that in both geometries, the ore/coke ratio is low at the furnace centre, and coke particle size is small near the furnace wall. This burden distribution provides high permeability at the furnace centre due to large particles causing large voids for fluid flow.

During descent: 1) the particle properties at the top of the furnace are transported to other parts of the furnace with the solid streamlines so as to initialize particle size and porosity distributions throughout the furnace. 2) After identifying the cohesive zone, dripping zone and deadman, the properties of these regions are re-calculated as follows: i) in the cohesive zone, porosity and particle size of iron ore are a function of normalized shrinkage ratio, Sh_r^*. Shrinkage ratio, Sh_r, is defined as the ratio of the decreased volume, due to softening and melting, to the original volume occupied by iron ore; ii) in the dripping zone, bed permeability is calculated based on coke size only; iii) in the deadman, coke particle size (0.02 m) and solid fraction (0.65) are assumed constant.

2.3.3 Treatment of cohesive zone

In practice, the cohesive zone shape and position will determine the permeability, fluid flow, gas utilization, thermal and chemical efficiency and hot metal quality in the furnace. Numerically, the cohesive zone is usually defined to start and finish within the solid temperature range of 1,200°C-1,400°C. The numerical treatment of a cohesive zone may be isotropic, anisotropic non-layered or layered.[15] Since the details of multiphase flow and relevant thermo-chemical behaviours inside the cohesive zone are not the scope of this study, the isotropic treatment is adopted in this model for simplicity, where the cohesive zone is treated as a mixed region of iron ore and coke particles (Table 5).

Table 5. Treatment of cohesive zone used in the study

Parameters	Treatment
Solid volume fraction	$\varepsilon_s = \xi_{ore}\varepsilon_{ore} + \xi_{coke}\varepsilon_{coke}$
Solid particle size	$d_s = (\xi_{ore}/d_{ore} + \xi_{coke}/d_{coke})^{-1}$
Solid heat conductivity	$k_s = (\xi_{ore}/k_{ore} + \xi_{coke}/k_{coke})^{-1}$
Gas flow resistance in cohesive zone	$\alpha_f = 1.75\frac{1-\varepsilon_s}{d_s}$ $\beta_f = 150\frac{\mu_g(1-\varepsilon_s)^2}{d_s^2\varepsilon_s}$

2.3.4 Solution procedure

The solution procedure employed in this CFX-based model is outlined below: 1) A pre-calculation of mass balance is conducted outside of CFX runs for determining boundary conditions and initial conditions; 2) The respective CFX runs of gas-solid-liquid phases are conducted for calculating their flow-thermal-chemical behaviours. This will lead to a determination of the cohesive zone; 3) The shared library is

ISSN 2176-3135

updated by repeating step 2 for the three phases until the difference in relative cohesive zone positions predicted by two consecutive iterations is less than 10%.

3 RESULTS AND DISCUSSION

3.1 Effect of Slot and Sector Geometries on Cohesive Zone

Figure 2a shows the effect of sector/slot geometry on the location and shape of the cohesive zone. The simulations show that compared with the slot geometry, the predicted cohesive zone is located at a similar height at furnace centre but higher at the furnace wall using the sector geometry, *i.e.* a flatter-shaped cohesive zone at a higher position is predicted. The reason for the difference can be explored as follows: Under the same burden distribution conditions at the furnace top, the sector geometry will have more large particles near the belly wall (Figure 2b), and the majority of them are coke (Figure 4b). This will lead to a larger bed voidage and then a higher solid temperature near the belly wall (Figure 4a). This will be discussed further below. It can be inferred that the choice of a slot or sector model geometry in BF modelling will affect the cohesive zone shape and location significantly and thus cannot be ignored when examining the multiphase behaviours inside a BF.

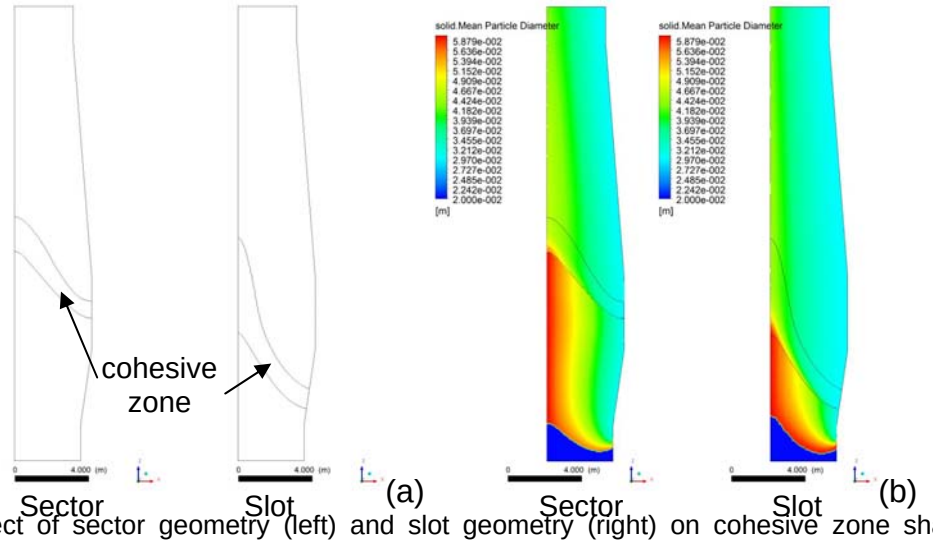

Figure 2. Effect of sector geometry (left) and slot geometry (right) on cohesive zone shape and location (a) and particle size (b).

3.2 Effect of Slot and Sector Geometries on Key Process Variables

3.2.1 Velocity fields of gas/solid phases

Figure 3 shows the solid volume fraction and effect of sector/slot geometries on the velocity fields of solid and gas phases. The simulations indicate that the regions of a BF (Figure 3a), *i.e.* lumpy zone, cohesive zone, dripping zone (coke bed) and solid stagnant zone (deadman), show different profiles in the predictions by the two geometries *i.e.* higher cohesive zone as discussed above and also a slightly lower deadman profile predicted in the sector geometry. Such difference will affect the solid and gas velocity fields significantly: i) in each case, the solid velocities decrease after reaching the cohesive zone (located higher in the sector model) and decrease further after reaching the deadman (located lower in the sector model). That is, the sector geometry predicts an earlier decrease of solid velocity. ii) The gas velocities are different in different regions: after entering the BF via tuyeres, the gas velocity

ISSN 2176-3135

decreases and is redirected significantly after reaching the deadman (located lower in the sector model) and then further decreased and redirected slightly after reaching the cohesive zone (located higher in the sector model).

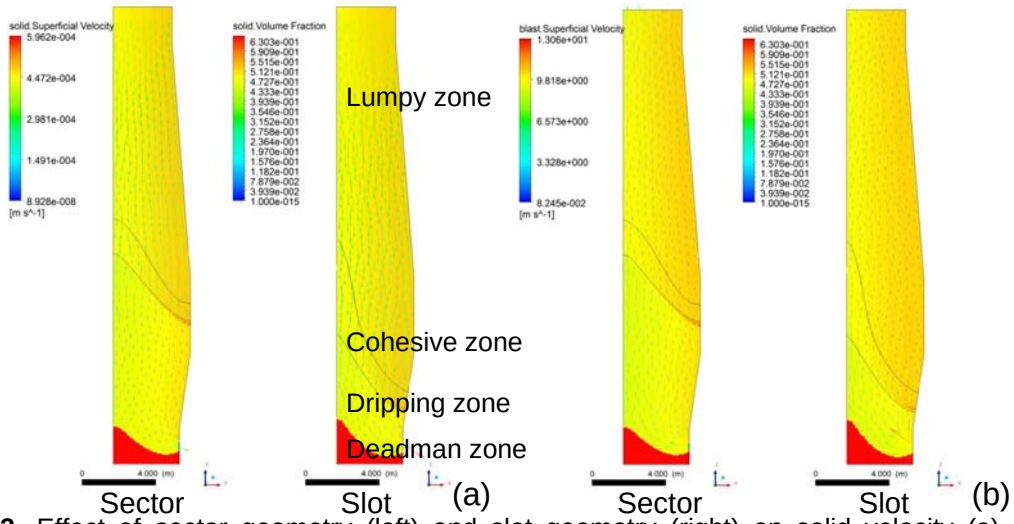

Figure 3. Effect of sector geometry (left) and slot geometry (right) on solid velocity (a) and gas velocity (b).

3.2.2 Solid temperature and component concentration

Figure 4a shows the effect of sector/slot geometries on solid temperature. The simulations indicate that in both cases, during descent through these regions, the solids are heated gradually followed by a much faster change at the lower boundary of the cohesive zone. The sector geometry predicts a higher solid temperature near the wall of furnace belly, leading to a higher cohesive zone. The gas temperature shows the similar trend.

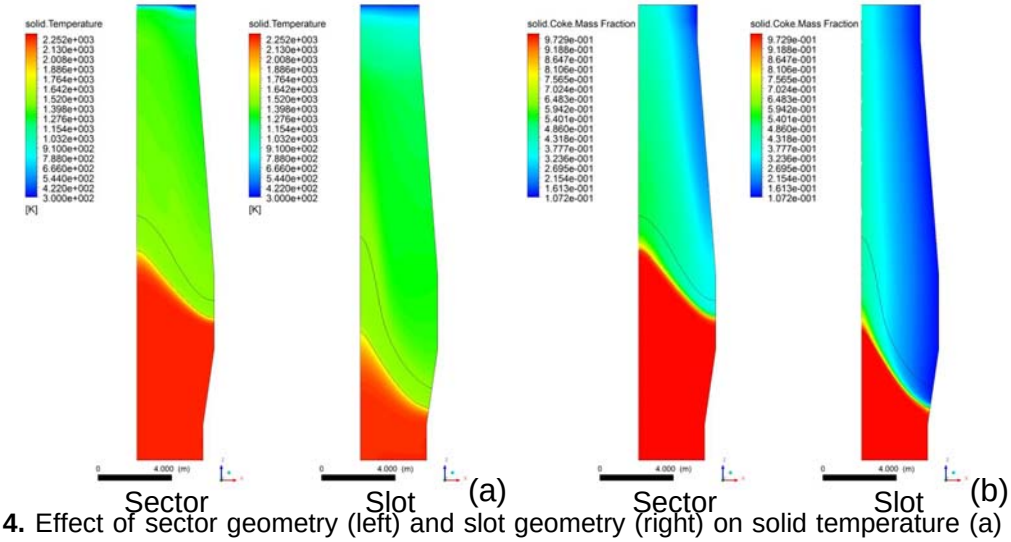

Figure 4. Effect of sector geometry (left) and slot geometry (right) on solid temperature (a) and coke mass fraction (b).

Figure 4b shows the effect of sector/slot geometries on the coke mass fraction of the solids. The simulations indicate that more coke is observed near the furnace centre than near the wall in both cases. On the other hand, the coke mass fraction is also significantly affected by the different geometries: the dripping zone with 100% coke is

ISSN 2176-3135

larger in the sector geometry. More coke is observed near the belly wall in the sector geometry from the combined effect of flow and various chemical reactions.

3.2.3 Liquid flow

Figure 5 shows the effect of sector/slot geometries on liquid velocity superimposed on solid volume fraction (a) and liquid volume fraction (b). The simulations indicate that liquids are generated at a higher position *i.e.* earlier liquid generation, in the sector geometry. The liquid streams percolate through the coke bed in the dripping zone and then enter the deadman, which is located at a slightly lower position in the sector model. Liquid flow is then deflected in front of the tuyeres due to gas-liquid interaction, resulting in a region of higher volume fraction inward from the wall.

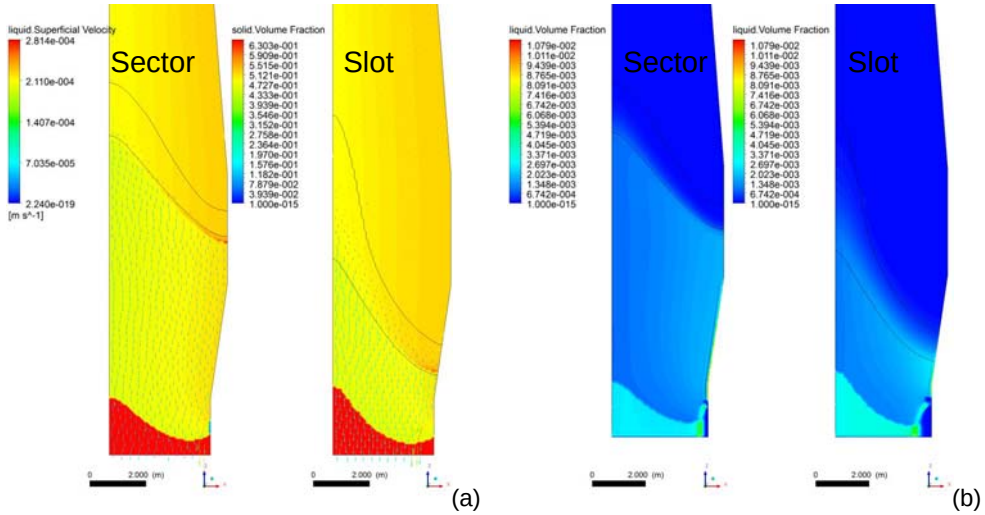

Figure 5. Effect of sector geometry (left) and slot geometry (right) on liquid flow: liquid velocity (a) and liquid volume fraction (b).

3.2.4 Other process variables

Figure 6 shows the effect of sector/slot geometries on reduction degree (f_s) and gas utilization. The simulations indicate that the sector geometry predicts earlier or faster ore reduction in the lumpy zone, especially near the wall in the furnace shaft. This is consistent with the cohesive zone predictions. The gas utilization, defined as $CO_2/(CO_2+CO)$ is also investigated as it represents the efficiency of reducing gas in the furnace shaft to a certain degree. The gas utilization at the furnace top is ~48.5% in the sector model and ~54.2% in the slot model, *i.e.* reducing gas is used at a lower efficiency in the prediction using the sector geometry.

ISSN 2176-3135

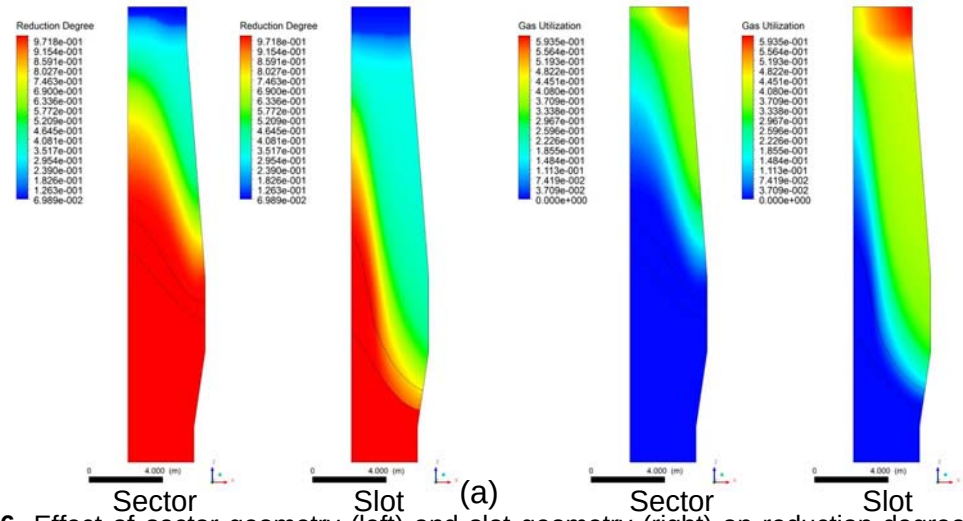

Figure 6. Effect of sector geometry (left) and slot geometry (right) on reduction degree (a) and gas utilization (b).

4 CONCLUSIONS

A CFX-based CFD model is developed to describe the internal state of a BF in terms of fluid flow, heat and mass transfer, and chemical reactions. The model is used to investigate and visualise the effects of different model geometries, *i.e.* slot geometry and sector geometry, on the simulations including location/shape of the cohesive zone and other key process variables such as fluid velocity, temperature, component concentration of each phase, reduction degree and gas utilization. The model provides a cost-effective method for understanding and optimizing the BF operation.
The comparisons show that predictions of fluid flow and thermo-chemical phenomena using the slot geometry and sector geometry are quiet different: (1) The sector geometry predicts a higher cohesive zone location near the furnace wall; (2) The sector geometry predicts a higher solid temperature and a higher coke mass fraction near the furnace wall, earlier liquid generation, a faster reduction process, and a lower gas utilization at the furnace top. This implies that model geometry exerts a significant influence on predictions and thus should be used with caution when numerically examining the multiphase behaviours inside a BF.

Acknowledgements

The authors are grateful to the Australian Research Council and BlueScope Steel for the financial support of this work, and to Dr X.F. Dong and Dr D. Pinson (BlueScope Steel) and Dr S. B. Kuang (UNSW) for valuable discussion.

REFERENCES

1 Omori, Y., *Blast Furnace Phenomena and Modelling*. Elsevier Applied Science: London; New York, 1987.
2 Yagi, J. Mathematical modeling of the flow of four fluids in a packed bed. *ISIJ International,* v. 33, p. 619-639, 1993.
3 Shen, Y. S.; Maldonado, D.; Guo, B. Y.; Yu, A. B.; Austin, P.; Zulli, P. Computational fluid dynamics study of pulverized coal combustion in blast furnace raceway. *Industrial & Engineering Chemistry Research,* v. 48, p. 10314-10323, 2009.
4 Shen, Y. S.; Guo, B. Y.; Yu, A. B.; Austin, P. R.; Zulli, P. Three-dimensional modelling of in-furnace coal/coke combustion in a blast furnace. *Fuel,* v. 90, p. 728-738, 2011.

ISSN 2176-3135

5 Dong, X. F.; Yu, A. B.; Yagi, J.; Zulli, P. Modelling of multiphase flow in a blast furnace: recent developments and future work. *ISIJ Int.,* v. 47, p. 1553-1570, 2007.
6 Ueda, S.; Natsui, S.; Nogami, H.; Yagi, J.; Ariyama, T. Recent Progress and Future Perspective on Mathematical Modeling of Blast Furnace. *ISIJ International,* v. 50, p. 914-923, 2010.
7 ANSYS-CFX-Documentation In.
8 Guo, B. Y.; Zulli, P.; Daniel, M.; Yu, A. B.; Shen, Y. S. Modelling of titanium compound formation in blast furnace hearth. *Journal of Iron and Steel Research International,* v. 16, p. 851-856, 2009.
9 Yagi, J. Mathematical modeling of the flow of four fluids in a packed bed. *ISIJ Int.,* v. 33, p. 619-639, 1993.
10 Austin, P. R.; Nogami, H.; Yagi, J. A mathematical model of four phase motion and heat transfer in the blast furnace. *ISIJ Int.,* v. 37, p. 458-467, 1997.
11 Wang, G. X.; Chew, S. J.; Yu, A. B.; Zulli, P. Modeling the discontinuous liquid flow in a blast furnace. *Metallurgical and Materials Transaction,* v. 28B, p. 333-343, 1997.
12 Chew, S. J.; Zulli, P.; Yu, A. B. Modelling of liquid flow in the blast furnace: theoretical analysis of the effects of gas, liquid and packing properties. *ISIJ Int.,* v. 41, p. 1112-1121, 2001.
13 Hatano, M.; Miyazaki, T.; Iwanaga, Y. Mathematical-model for blast-furnace operation considering the degradation of coke by gasification. *Transactions of the Iron and Steel Institute of Japan,* v. 20, p. 292-300, 1980.
14 Austin, P. R.; Nogami, H.; Yagi, J. A mathematical model for blast furnace reaction analysis based on the four fluid model. *ISIJ Int.,* v. 37, p. 748-755, 1997.
15 Dong, X. F.; Yu, A. B.; Chew, S. J.; Zulli, P. Modeling of Blast Furnace with Layered Cohesive Zone. *Metallurgical and Materials Transactions B-Process Metallurgy and Materials Processing Science,* v. 41, p. 330-349, 2010.
16 Austin, P. R.; Nogami, H.; Yagi, J. A mathematical model of four phase motion and heat transfer in the blast furnace. *ISIJ International,* v. 37, p. 458-467, 1997.

NOMENCLATURE

a_{FeO}	the activity of molten wustite	***Greek***	
A_c	effective surface area of coke for reaction, m^2	Γ	diffusion coefficient
$A_{sl,d}$	effective contact area between solid and liquid in unit volume of bed, $m^2 \cdot m^{-3}$	**I**	identity tensor
c_p	specific heat, $J \cdot kg^{-1} \cdot K^{-1}$	ϕ	general variable
d	diameter of solid particle, m	φ	shape factor
d_w	effective packing diameter, m	α_f, β_f	coefficients in Ergun Eq.
D	diffusion coefficient, $m^2 \cdot s^{-1}$	β	mass increase coefficient of fluid phase associated with reactions, $kg \cdot mol^{-1}$
E_f	effectiveness factors of solution loss reaction	ε	volume fraction
f_s	degree of reduction	μ	viscosity, $kg \cdot m^{-1} \cdot s^{-1}$
f	interaction force per unit volume, $kg \cdot m^{-2} \cdot s^{-2}$	ρ	density, $kg \cdot m^{-3}$
$f(d_{coke})h(S_L)$	correction factors for particle size and coke reactivity	τ	stress tensor, Pa
g	gravitational acceleration, $m \cdot s^{-2}$	ξ_{ore}, ξ_{coke}	local ore, coke volume fraction
h	holdup	ξ_i	mass fraction of species *i*
$h_{l,t}$	total holdup	***Subscripts***	

ISSN 2176-3135

h_{ij}	heat transfer coefficient between i and j phase, $W \cdot m^{-2} \cdot K^{-1}$	*e*	effective
H	enthalpy, $J \cdot kg^{-1}$	*g*	gas
k	thermal conductivity, $W \cdot m^{-1} \cdot K^{-1}$	*i*	identifier (g, s or l)
k_f	gas-film mass transfer coefficient, $m \cdot s^{-1}$	*i,m*	mth species in i phase
k_i	rate constant of ith chemical reactions (i = 1, 2 or 3), $m \cdot s^{-1}$	*j*	identifier (g, s or l)
K	equilibrium constant	*k*	kth reaction
M_i	molar mass of ith species in gas phase, $kg \cdot mol^{-1}$	*l*	liquid
$\overline{M}_g$	molar mass of gas mixture, $kg \cdot mol^{-1}$	*l,d*	dynamic liquid
N_{ore}	number of ore particles per unit volume of bed, m^{-3}	*s*	solid
p	pressure, Pa	*sm*	FeO or flux in solid phase
R	gas constant, 8.314 $J \cdot K^{-1} \cdot mol^{-1}$	***Superscripts***	
R^*	reaction rate, $mol \cdot m^{-3} \cdot s^{-1}$	*e*	effective
S	source term	*g*	gas
Sh_r^*	normalized shrinkage ratio, $Sh_r^* = Sh_r / Sh_{r,\max}$, $Sh_{r,\max} = 0.7$	*l,d*	dynamic liquid
T	temperature, K	*s*	solid
U	true velocity, $m \cdot s^{-1}$	T	total
V_b	bed volume, m^3		
V_g	gas volume, m^3		
Vol_{cell}	volume of control volume, m^3		
y_i	mole fraction of i^{th} species in gas phase		